Sheffield Hallam University

Investigation of aqueous slurry erosion-corrosion behaviour of Tantalum in different pH solutions
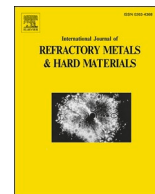
CHOUHAN, Jitendra, PURANDARE, Yashodhan <http://orcid.org/0000-0002-7544-9027>, JANA, Buddhadev, DEY, A., HOVSEPIAN, Papken <http://orcid.org/0000-0002-1047-0407>, JENKINS, D. and JONES, L.

Citation:

Copyright and re-use policy

Investigation of aqueous slurry erosion-corrosion behaviour of Tantalum in different pH solutions

J.S. Chouhan [a], Y.P. Purandare [a,*], B.D. Jana [a,b], A. Dey [c], P.Eh. Hovsepian [a], D. Jenkins [c], L. Jones [c]

[a] Materials and Engineering Research Institute, Sheffield Hallam University, City Campus, Howard Street, Sheffield S1 1WB, United Kingdom
[b] Department of Engineering and Mathematics, Sheffield Hallam University, City Campus, Howard Street, Sheffield S1 1WB, United Kingdom
[c] Rutherford Appleton Laboratory, Didcot OX11 0QX, United Kingdom

ARTICLE INFO

ABSTRACT

Erosion-corrosion behaviour of pure Tantalum (Ta) was investigated using corrosive slurry solutions (pH 4, 7, and 10) containing 7 wt% SiC as erodent particles. Tests were carried out using an impinging jet erosion-corrosion apparatus with a jet velocity of 5 ms^{-1} and at two impact angles (30° and 90°). Under particle bombardment conditions, a marked reduction in corrosion resistance offered by Ta was observed amid a significant cathodic shift in the E_{Corr} values for all pH values investigated. Results showed that interaction between erosion and corrosion was higher under 30° impact leading to a higher rate of material removal. On the contrary, negative synergism was observed for experimental conditions of normal impact for pH 7 and pH 10. Scanning electron microscopy studies revealed typical ductile erosion mechanisms of material removal which consisted of dominating micro-cutting for 30° and plastic deformation resulting in lip formation for normal impact angle. These appeared to be assisted by dissolution of weakened areas and passive layer removal as corrosion mechanisms. Potentiostatic erosion-corrosion experiments were utilised for calculation of synergistic and antagonistic effects and have been presented in the paper.

1. Introduction

Tantalum (Ta) has a high melting point and high corrosion resistance owing to its ability to instantaneously grow a non-porous oxide layer, mainly Ta_2O_5, due to a high affinity towards oxygen [1]. In addition, with a heavy nucleus, a higher neutron yield and good solid solubility with Tungsten (W), it forms a commendable choice of water-cooled cladding that is diffusion bonded on spallation targets especially made from Tungsten [2–4]. Prima facie, Ta clad W spallation target design approach looks promising and is currently being used at ISIS (neutron scattering facility at STFC Rutherford Appleton Laboratory (RAL), UK). However, the Hot Isostatic Pressing (HIP) diffusion bonded Ta—W spallation target is currently experiencing a premature failure that is significantly reducing its operation life [5].

Apart from being tough and very ductile, the hardness of Ta, depending on the route of manufacturing, is in the range of 60–200 HV and compares to that of mild steel or age-hardened aluminium alloys [6–8]. As a consequence of irradiation, a hardness increase of up to 3

times as compared to that of unirradiated Ta has also been reported [9,10]. With this backdrop, it is possible that, because of irradiation-induced stresses, high temperature, embrittlement and or cracking of the Ta—W diffusion bonded target or the protective passive oxide layers of Ta may occur releasing loose debris in the closed-circuit cooling water loop. Previous work at Rutherford Appleton Laboratory (RAL) found radioactive isotopes of ^{172}Lu, ^{175}Hf, ^{187}W and ^{182}Ta in the cooling water loop along with its pH value changes [5] suggesting that loose solid particles, mainly associated with the disintegration of Ta, may have been circulating along with the cooling water. Thus, giving rise to a scenario that Ta may have been subjected to aqueous slurry erosion and erosion-corrosion conditions.

Aqueous slurry erosion (solid particles suspended in a liquid) of pure Ta, and especially of Ta manufactured via Powder Metallurgy (PM) route is poorly understood since very little literature on the erosion of Ta exists. A previous publication [8] from the authors carried out a systematic evaluation of the slurry erosion behaviour of PM-manufactured Ta in deionised water (in the absence of corrosion). As anticipated from

the hardness values, Ta exhibited a typical ductile material erosion response [11,12] with higher erosion rates at an oblique (30°) impact angle rather than at higher impact angles in the range of 60° to 90°. Micro-cutting and ploughing resulted in platelets/ lips formation at oblique impact angles whereas breakage of lips due to repeated erodent particle bombardment at angles close to normal impact was identified as the main mechanism of material removal [8]. The mechanism was also found to be assisted by the formation of extensive voids/cavities all over the eroded surface [8].

Aqueous slurry erosion-corrosion (henceforth termed erosion-corrosion in the text) can be termed a process of wear involving progressive loss of material due to the combined action of mechanical erosion and chemical corrosion [13]. In erosion-corrosion, there is a complex interplay between erosion and corrosion which results in an additive effect when erosion enhances corrosion or a synergistic effect when corrosion enhances erosion [14–16]. Literature on the slurry erosion-corrosion analysis of pure Ta is virtually non-existent and hence demands systematic laboratory studies to form the first few building blocks (without radiation effects) of the approach to solve the problem faced at RAL. This work reports the results of laboratory-based impinging jet erosion-corrosion tests performed on pure Ta manufactured via PM route. Accelerated tests have been performed using slurries made of SiC abrasive particles and corrosive solutions with different pH values.

2. Experimental

2.1. Specimens

Ta samples used in the study were manufactured through the PM route. They consisted of cylindrical shaped discs, 30 mm diameter and 5 mm thick (hardness value of 89 ± 3 HV$_2$), which represents the material

spallation targets at RAL. Slurries were prepared by mixing angular Silicon Carbide (SiC) particles of hardness in the range of 22–25 GPa and with an average size of 500–710 μm in buffer solutions with a 7 ± 1 wt% concentration. Cooling water analysis at the site (RAL) indicated pH value changes, from initial value of pH 7 (demineralised water) to acidic values with passage of time [5]. However, to gain a comprehensive view of the material performance in different corroding conditions, buffer solutions with three pH values; namely 4, 7 and 10 were chosen. Table 1 provides the details of the buffer solutions. The design of the specimen holder facilitated exposing a fixed area (0.33 cm^2) on a masked sample held in front of the exit nozzle (of 6.5 mm diameter) at a distance of 15 mm.

A computer-controlled potentiostat (ACM Gill AC) was used to maintain and monitor the corrosion response of the specimens under simultaneous particle bombardment. A saturated Ag/AgCl electrode was used as a Reference Electrode (RE) whereas a graphite rod was used as an Auxiliary Electrode (AE) to form a standard 3-electrode electrochemical cell with the exposed specimen forming the Working Electrode (WE) [17]. All electrochemical potentials reported in this article henceforth are with respect to the Ag/AgCl reference electrode.

In order to analyse the effect of erosion on corrosion, flow corrosion experiments (5 ms^{-1}) were performed with and without particles and under potentiodynamic (potential sweep from -1 V to +1 V rate of 0.6 mVs^{-1}) and potentiostatic conditions (representing anodic dissolution conditions derived from the polarisation curves). All experiments were performed according to ASTM G119–09 standard [18] at ambient temperatures (22–24 °C), had a fixed duration of 1 h and were repeated 3 times to analyse their reproducibility. After each experiment, the specimens were dried and weighed using a precision balance with the least count of 0.0001 g. The erosion-corrosion rate (K_{ec}) is calculated as follows:

$$\text{sample mass loss}, \text{m (g)} = \text{initial sample mass–final sample mass (after 1 h experiment)}$$

used for the cladding albeit without the microstructure affected by irradiation or by the Hot Isostatic Pressing technique (HIP) used for diffusion bonding of Ta cladding to the W target. All samples were metallurgically polished to a mirror finish before being subjected to an impinging jet of corrosive slurry. Details of the Ta specimen polishing, mechanical and microstructural characterisation can be found in the previous publication [8].

2.2. Impinging jet aqueous erosion-corrosion experiments

The accelerated slurry erosion-corrosion experiments were performed with the help of an impinging jet erosion-corrosion apparatus based at Sheffield Hallam University. Details of the apparatus have been included in the previous publication [8]. Depending on the feedback from the previous studies, experiments were carried out at two impact angles; namely at 30° which exhibits a peak in pure slurry erosion rate and at 90°, in ambient conditions (20–22 °C temperature). Slurry velocity and concentration were maintained constant at 5 ms^{-1} and represent an intermediate water circulation rate used for cooling the

$$\text{mass loss per } sec, \text{m}_{ec} \text{ (kg s}^{-1}) = \text{m}/(3600 \times 1000) \quad (1)$$

$$\text{mass loss rate per unit area}, K_{ec} = \text{m}_{ec}/A \quad (2)$$

where,

$$\text{sample exposed area}, A = (\pi/4) \times D^2 = 0.332 \text{ cm}^2 \quad (3)$$

where D is the sample exposed zone diameter (6.5 mm).

Combining Eq. 1–3 gives,

Table 1
Corrosive solutions used in the erosion-corrosion apparatus.

Type of solution	pH
0.5 M Citrate Buffer (Citric Acid and Sodium Citrate Dihydrate)	4
0.5 M Sodium Chloride	7
0.5 M Carbonate Buffer (Sodium Carbonate and Sodium Bicarbonate)	10

Table 2
Operating conditions for erosion, corrosion, and erosion-corrosion tests.

	Erosion	Corrosion	Erosion-corrosion
Impact angle (°)	30, 90	30, 90	30, 90
Impact velocity (ms^{-1})	5	5	5
SiC concentration (wt%)	7	–	7
Test duration (h)	1	1	1
Solution (0.5 M)	Deionised water	Citrate buffer, Sodium chloride, Carbonate buffer	Citrate buffer, Sodium chloride, Carbonate buffer
Temperature (°C)	22–24	22–24	22–24

Table 3
Operating parameters for potentiostatic experiments.

Impact angle (°)	Set potential (mV):		
	pH 4	pH 7	pH 10
30	+ 230	− 125	+ 111
90	+ 60	− 80	− 35

$$K_{ec} \left(kg\ m^{-2}\ s^{-1}\right) = m_{ec} / \left(0.332 \times 10^{-4}\right)$$

$$= m / \left(3600 \times 1000 \times 0.332 \times 10^{-4}\right)$$

$$= m / 119.52$$

The corrosion current density was obtained from the Tafel plot by extrapolating anodic and cathodic branches of the potentiodynamic polarisation scan and determining the point of intersection [19]. Table 2 and Table 3 shows a summary of experimental conditions used in this investigation.

3. Results and discussion

3.1. Effect of particle bombardment on polarisation curves

It is well established that wear (mechanical damage caused by particle bombardment) has a pronounced effect on the corrosion performance of passive metals and alloys. The most influential effect, depending on the impact energy of particles and properties of the surface in question, is the removal of surface oxides and passive layers leading to the exposure of fresh surface beneath it to the corrosive liquid. Removal of these protective layers leads to an increment in corrosion rate until it repassivates again [13].

Fig. 1a shows the polarisation curves obtained when the specimens were inclined at 30° to the incoming jet (corrosion-only conditions). As observed, the pH value of the solution had a significant effect on the E_{Corr} value. Among the test conditions employed in this study, the most noble E_{Corr} value (−0.064 ± 0.01 V) was observed when tested against Citric buffer solution (pH 4), followed by Sodium carbonate buffer solution (pH 10; E_{Corr} value of −0.170 ± 0.01 V). The least noble E_{Corr} value of −0.358 ± 0.01 V was observed for 3.5% NaCl solution with a pH value of 7.

Ta surface is characterised by the formation of protective Ta_2O_5 passive layers (in the range of a few nanometres, [20]. In this case, Ta specimens can be visualised as one possessing a thin coating (few nm) of Ta_2O_5 on the top. Thus, E_{Corr} and corrosion density values recorded in this case (corrosion under flow conditions without particles) were of the "coated" Ta specimens. Polarisation results suggested that in anodic conditions, corrosion of the specimen proceeded either by removal of the inherent passive layer by the flowing solution and/or dissolution of the passive layer/substrate.

Fig. 1b shows the polarisation curves obtained during the impingement of corrosive slurry (impact angle of 30°). A marked reduction in corrosion resistance was observed, wherein a significant cathodic shift in the E_{Corr} values (in the range of 400–500 mV) was observed (Table 4) for all pH values. This negative shift in the E_{Corr} values could be attributed to the removal of the inherent passive layer due to particle bombardment and is akin to the negative shift observed in OCP values observed for passive metals in tribocorrosive conditions [21]. As the anodic potentials increased from −250 mV to +1000 mV, current densities increased steadily, albeit with little difference in the shape and slope of the curves for different pH values. This indicated that material removal through particle bombardment (mechanical component) was dominating, and it suppressed the repassivation of the surface to a large extent.

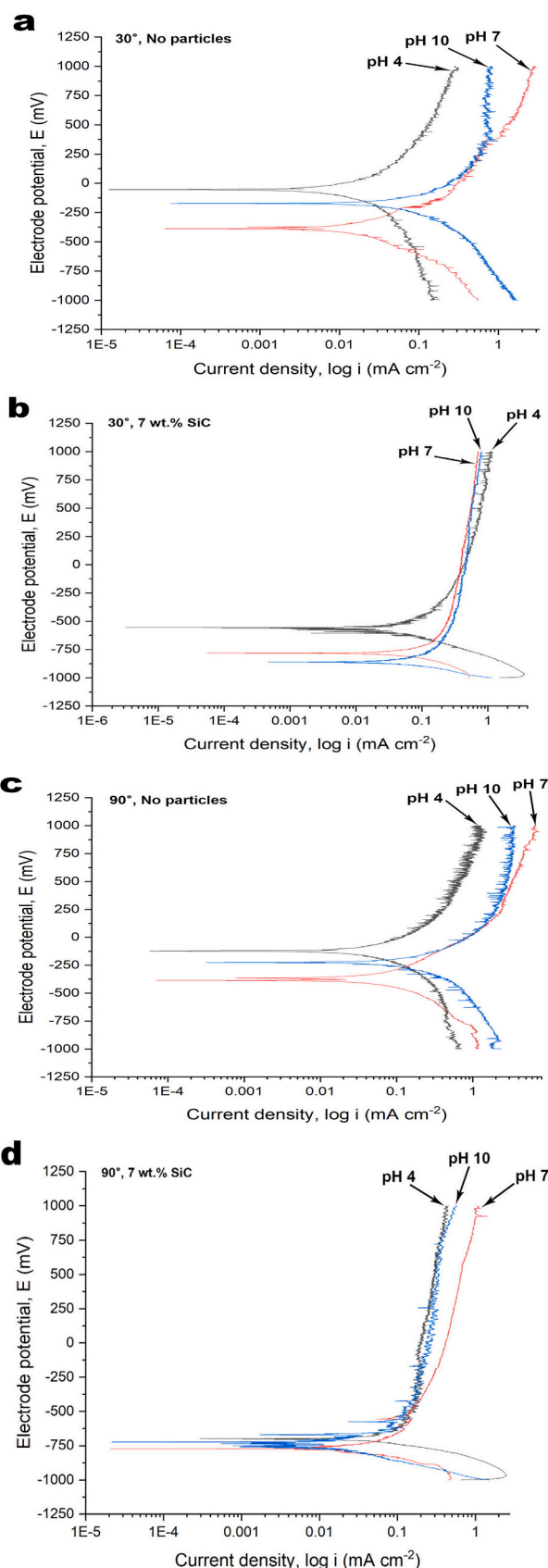Fig. 1c and d show the polarisation curves obtained when the

Fig. 1. Polarisation curves obtained for Tantalum in pH 4, pH 7, and pH 10 solutions impinging at 5 ms^{-1} velocity (a) without particles at 30° impact angle, (b) with 7 wt% SiC particles at 30° impact angle, (c) without particles at 90° impact angle, (d) with 7 wt% SiC particles at 90° impact angle.

Table 4
Mean corrosion potentials and current densities obtained from polarisation curves at different pH and impact angles.

Operating parameters	pH	Corrosion potential E_{Corr} (V)	Corrosion current density i_{corr} (μA cm^{-2})
	4	-0.064 ± 0.01	9 ± 1.70
30°, No SiC	7	-0.358 ± 0.03	17 ± 1.99
	10	-0.170 ± 0.01	163 ± 0.91
	4	-0.593 ± 0.08	23 ± 2.49
30°, 7 wt% SiC	7	-0.780 ± 0.01	57 ± 4.99
	10	-0.871 ± 0.01	36 ± 2.94
	4	-0.127 ± 0.03	24 ± 1.89
90°, No SiC	7	-0.376 ± 0.02	66 ± 0.80
	10	-0.260 ± 0.02	116 ± 2.45
	4	-0.680 ± 0.01	33 ± 1.70
90°, 7 wt% SiC	7	-0.763 ± 0.01	60 ± 5.35
	10	-0.709 ± 0.02	15 ± 2.05

specimens were subjected to corrosive solutions (impinging at 90°) without and with the presence of abrasive particles respectively. A similar trend and near similar E_{Corr} values (Fig. 1c), as observed for pure corrosion experiments at 30° impingement (Fig. 1a) was also observed for 90° impingement (pure corrosion), suggesting that the impact angle did not play a significant role in determining E_{Corr} values in the absence of particle bombardment. When under abrasive slurry bombardment (Fig. 1d), a significant cathodic shift in the E_{Corr} values (also in the range of about 400–500 mV) was also observed for 90° impact angle, however, the difference in their absolute values for different pH solutions was less apparent. Our previous work [8] demonstrated that Ta shows a ductile erosion behaviour wherein, the maximum erosion rate was observed at low impact angles (30°) and the erosion rate decreased at higher impact angles. The results presented in Fig. 1d showed a clear influence of lower erosion rates at near-normal impact angles (for both passive layers and the base material) on the anodic current densities and could also be attributed to the mixed trends observed in the E_{Corr} values. The results suggested that the interaction (synergistic/additive) between erosion and corrosion process of material removal due to particle bombardment (mechanical component) was lower as compared to 30° impact conditions.

In the case of anodic current densities derived from Tafel slopes (Table 4), the trend observed was very mixed and unclear. A sharp increase in anodic dissolution corrosion current densities for erosion-corrosion as compared to corrosion-only conditions was observed for pH 4 and 7 at 30° impact. However, at pH 10, a significant reduction of corrosion current density as compared to corrosion-only conditions was observed and remains unexplained. Similarly, in general, corrosion

current densities at 90° impact (with and without particles) were higher for like-to-like conditions as compared to when impacted at 30°. The results suggested that the test geometries may have played a significant role in determining corrosion current densities. In corrosion-only conditions, at normal impact, the exposed specimen area would have seen the full brunt of the solution with a higher supply of corrosive species as compared to the 30° impact angle.

3.2. Erosion-corrosion rate

In order to investigate the erosion-corrosion rate (K_{ec}) and the effect of erosion on corrosion and vice versa, slurry erosion-corrosion as well as pure corrosion experiments were also performed at potentiostatic conditions (see Table 3) which represented passivating potentials (derived from the polarisation curves obtained for different pH values and impact angles, see Fig. 1). Pure erosion rates were derived from slurry erosion experiments performed in deionised water.

Fig. 2 shows the total erosion-corrosion rate (K_{ec}) obtained as a function of pH value and impact angles. As anticipated, K_{ec} values show a clear and strong dependency on impact angles, wherein an impact angle of 30° resulted in a higher K_{ec} rate as compared to the normal impact angle, and was in agreement with the ductile erosion behaviour of the same material (Ta manufactured through PM route) reported earlier [8]. The results for the 30° impact angle also exhibited a dependency on the pH value. The K_{ec} values for pH 7 and 10 were found to be lower as compared to pH 4. The significant rise in K_{ec} value ($K_{ec} = 3.47 \pm 0.2 \times 10^{-5}$) for pH 4 is noticeable, especially when under pure corrosion conditions, this pH value had the most noble E_{Corr} value (Fig. 1a). However, under passivating conditions, it also exhibited higher current densities under particle bombardment (potentials of 230 mV, Fig. 1b). These results indicate that the passive layer(s) formed in the potentials (range of -150 mV to 250 mV employed in this study) for pH 4 was inadequate in providing enough corrosion protection; was either porous or mechanically weak and was easily removed by particle bombardment. The K_{ec} value for pH 7 and pH 10 were in a similar range ($K_{ec} = 2.27 \pm 0.1 \times 10^{-5}$ and $1.98 \pm 0.1 \times 10^{-5}$) suggesting that passive layers formed under these conditions had similar electrochemical and physiomechanical properties. As a comparison, the mass loss due to erosion-corrosion was 3.3 times higher for pH 4, 2.2 times higher for pH 7 and 1.9 times higher for pH 10 than for pure slurry erosion conditions (mass loss values derived from the previous work conducted and presented in [8]).

The dependency of K_{ec} on pH for a 90° impact angle was less pronounced. At low impact angles ($< 45°$) the cutting mechanism dominates which results in higher removal of the material. For higher and
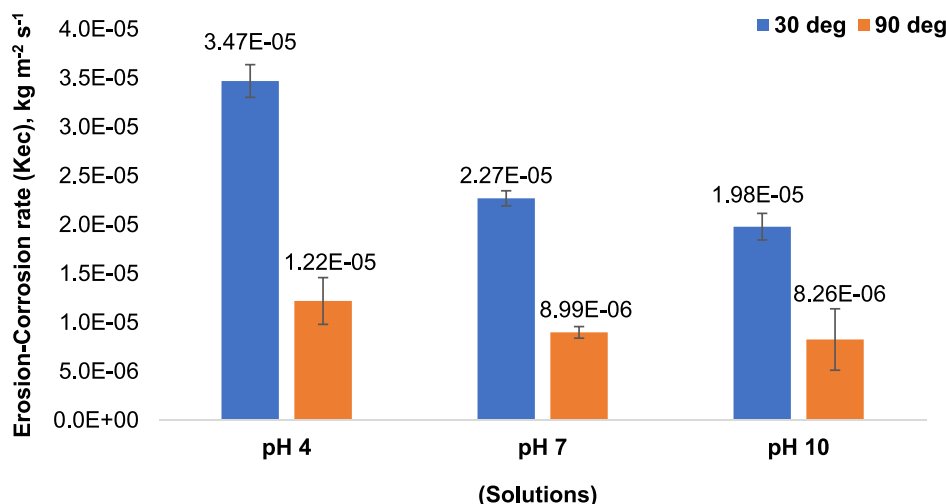

Fig. 2. Variation of Ta erosion-corrosion rate with various pH solutions at oblique and normal impact.

normal impact angles plastic deformation dominates, wherein repeated impacts are needed to dislodge material eventually by fatigue or fracture [11,22,23]. Also, a large amount of impact energy transfer could have led to a work-hardening effect [24]. Thus, the results from this study suggested that erosion of the surface layer(s), which includes any passive layers formed, was more efficient at a 30° impact angle than at 90°. Accordingly, K_{ec} values at 90° indicated a low dependency on pH value and that, damage induced by the bombarding particles was insufficient to remove the surface layers proficiently, thus reducing the interaction between erosion and corrosion. The results of potentiostatic experiments corresponded well with the polarisation experiments (Fig. 1). Unlike observed for 30° impact, the erosion-corrosion rate measured was almost similar to pure slurry erosion conditions for all respective pH values.

3.3. Erosion-corrosion mechanisms

The Fig. 3 shows SEM images of the wear scars after erosion-corrosion experiments when bombarded at 30° and 90° impact angles for the three pH solution slurries. Fig. 3a (pH 4), 3c (pH 7) and 3e (pH 10) show that scars were created when the particle impact angle was 30° whereas Figs. 3b (pH 4), 3d (pH 7) and 3f (pH 10) were created when the surface was impinged at 90°.

As a general consensus, the surface features observed on the wear scars were similar to those reported earlier for pure erosion of Ta [8] and frequently reported for ductile materials. No large scale grain dislodgement due to erosion or erosion assisted corrosion or vice versa and features associated with macro scale pitting was observed under any experimental set of conditions. As anticipated, the wear scars at 30° impact angles consisted of features such as extruded lips formed as a
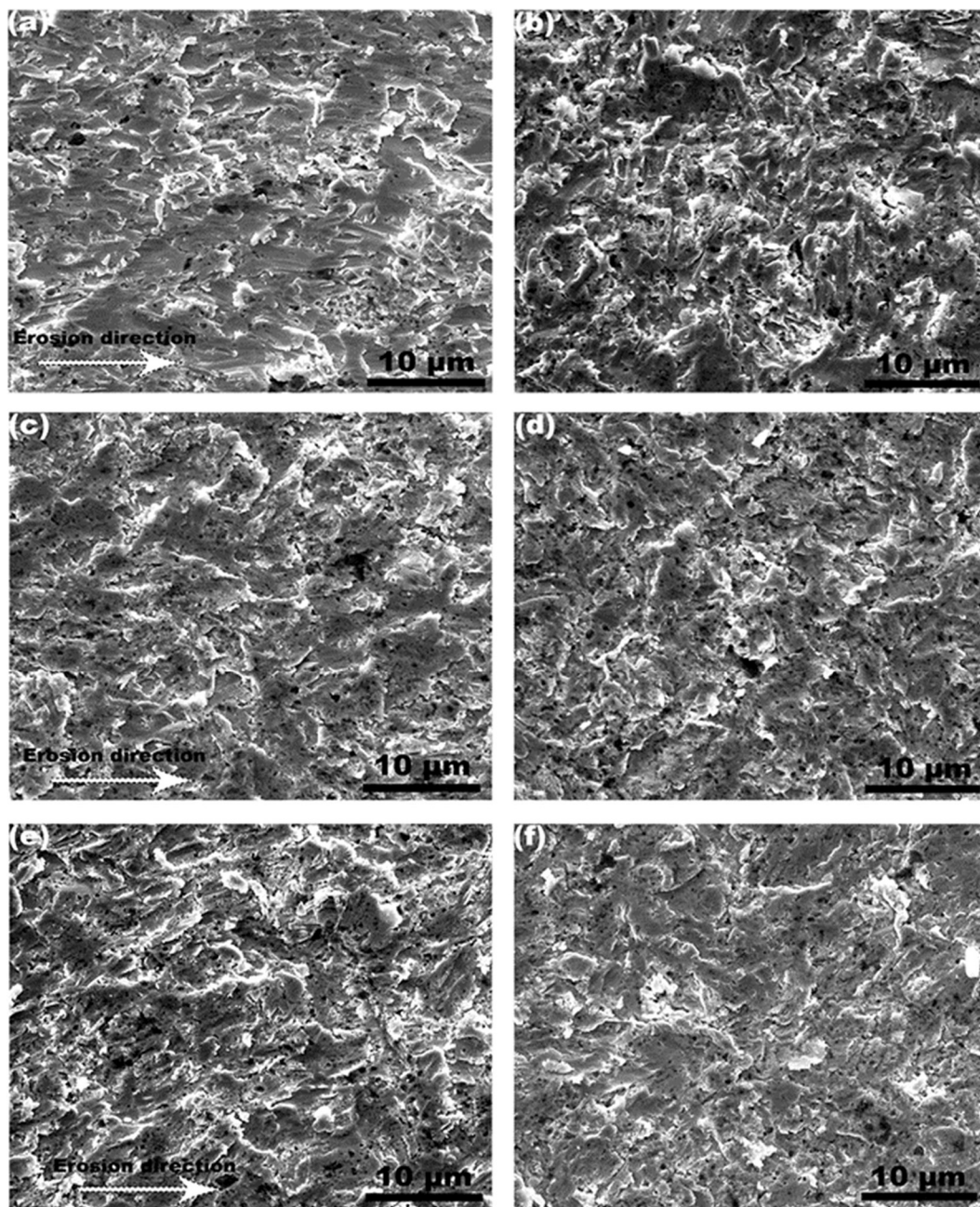

Fig. 3. SEM images of Ta after erosion-corrosion from various pH solution slurries (7 wt% SiC) at a jet velocity of 5 ms^{-1} at (a) 30° impact, pH 4 (b) 90° impact, pH 4 (c) 30° impact, pH 7 (d) 90° impact, pH 7 (e) 30° impact, pH 10 (f) 90° impact, pH 10.

result of ploughing action, as well as marks resembling Type-1 and Type-2 micro-cutting action [7]. The scars also exhibited extensive micro-sized voids and micro pitting resulting from the grain boundary sliding usually associated with lower strain rates [8]. Coalescence of these voids, lip fracture due to repeated particle impacts as well as grain dislodgement appeared to be the dominant material removal mechanism as far as the mechanical component was involved [8]. The pH value did not have a significant effect on these fundamentally, however, the wear scar for pH 4 (Fig. 3a) appeared a lot smoother compared to scars of pH 7 and 10 (both had near similar roughness, Fig. 3c and e respectively). Thus, an accelerated dissolution of the already weakened areas may have assisted the mechanical action of bombarding particles in dislodging the strained feature leading to a smoother finish (electro-polishing effect).

At 90° of impact angle, the wear scars showed typical features such as hills and valleys formed due to plastic deformation and breakage of extruded lips as reported earlier for Ta [8] and ductile type erosion of materials. The appearance of wear scar (roughness and extent of features) did not show any correlation with the pH value of the solutions. Extensive and ubiquitous micro-voids and pitting as was observed at 30° impact angle, were also visible for scars created at 90° of impact. Since the number, shape and sizes of the microvoids and pits formed in the wear scar were similar to those observed for pure erosion [8], for both impact angles and all solutions, the role of corrosion in their formation is very unclear.

3.4. Synergy

As a result of these effects between the mechanisms of erosion and corrosion, the total material loss can be higher than the sum of material loss due to each mechanism acting separately [16,25–27]. The synergy (ΔK_{ec}), which represents the enhanced wear rate of the material due to the unified action between erosion and corrosion [15], can be derived numerically using Eq. (4):

$$\Delta K_{ec} = K_{ec} - (K_{eo} + K_{co}) \tag{4}$$

where K_{ec} is the total wear rate due to erosion-corrosion, K_{eo} is the erosion rate due to pure erosion (i.e. with no corrosion contribution), K_{co} is the wear rate due to pure corrosion (i.e. with no erosion contribution).

The wear rate (synergy) ΔK_{ec} can be positive [24,28–30] or negative [31–33] and it is represented further using Eq. (5):

$$\Delta K_{ec} = \Delta K_e + \Delta K_c \tag{5}$$

where ΔK_e is the corrosion enhanced erosion rate (synergistic effect) and ΔK_c is the erosion enhanced corrosion rate (additive effect).

The Fig. 4 shows the synergy rate (ΔK_{ec}) calculated from eq. (4) for 30° and 90° impacts of various corrosive solutions. A significant positive synergy rate (expressed as kg m^{-2} s^{-1}) was observed for an impact angle of 30° at pH 4 (2.44×10^{-5}) which dropped for pH 7 (1.23×10^{-5}) followed by a further reduction for pH 10 (8.89×10^{-6}). In comparison, the synergy rate was an order of magnitude lower for a 90° impact angle for pH 4 (3.19×10^{-6}) and two orders of magnitude lower for pH 10 (-1.10×10^{-6}). For both pH 7 and pH 10, the corrosion appeared to have an antagonistic effect with negative synergy rates of -1.78×10^{-7} and -1.10×10^{-6} respectively.

The previous studies suggested that in an acidic solution the oxide film forms on the Ta surface according to the following electrochemical reaction [34–36],

$$2\,Ta + 5\,H_2O \rightarrow Ta_2O_5 + 10\,H^+ + 10\,e^- \tag{6}$$
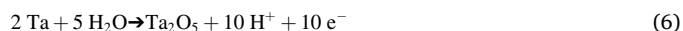
In alkaline solutions, on the Ta surface, the oxide layer formation takes place due to the following electrochemical reaction [34,37,38],

$$2\,Ta + 10\,OH^- \rightarrow Ta_2O_5 + 5\,H_2O + 10\,e^- \tag{7}$$
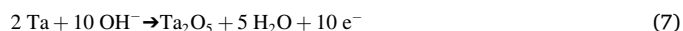
This Tantalum pentoxide (Ta_2O_5) layer provides passivity to the Ta surface under various electrode potentials [34]. Under pH 7 and pH 10, at an impact angle and velocity of 90° and 5 ms^{-1} respectively, these results suggest that the impact energy of the particles and the erosion mechanisms involved were insufficient to remove the protective layers present/formed on the Ta surface and that the rate of formation of this layer was higher than its rate of removal. As such, this oxide layer could have provided resistance to erosion by the impinging particles to some extent. In sharp contrast to the negative synergies of pH 7 and pH 10 solutions, a relatively high positive synergy rate at pH 4 suggested a weaker surface protection.

Fig. 5 and Fig. 6 show erosion enhanced corrosion rate and corrosion enhanced erosion rate respectively for various pH solutions at oblique and normal impact. The results suggested that for normal impact, the erosion enhanced corrosion rate (ΔK_c) values were higher than the corrosion enhanced erosion rate (ΔK_e) values in various pH solutions. At oblique impact, ΔK_e values were considerably higher than ΔK_c values in all solutions. In Fig. 5 the additive effect (erosion enhanced corrosion rate, ΔK_c) decreased as the solution became more alkaline at both 30° and 90° impact angles. The suppressed erosion enhanced corrosion rate is due to the formation of protective surface layers on Ta in alkaline solutions as discussed earlier due to the quick repassivation of the freshly exposed areas (and thickening of undisturbed passive layers). Under both impact angles, the synergistic effect, or the corrosion enhanced erosion rate (ΔK_e) follows a similar trend as that of variation in synergy rate (Fig. 4) of decrease in value as the solution became more alkaline from pH 4 to pH 10.
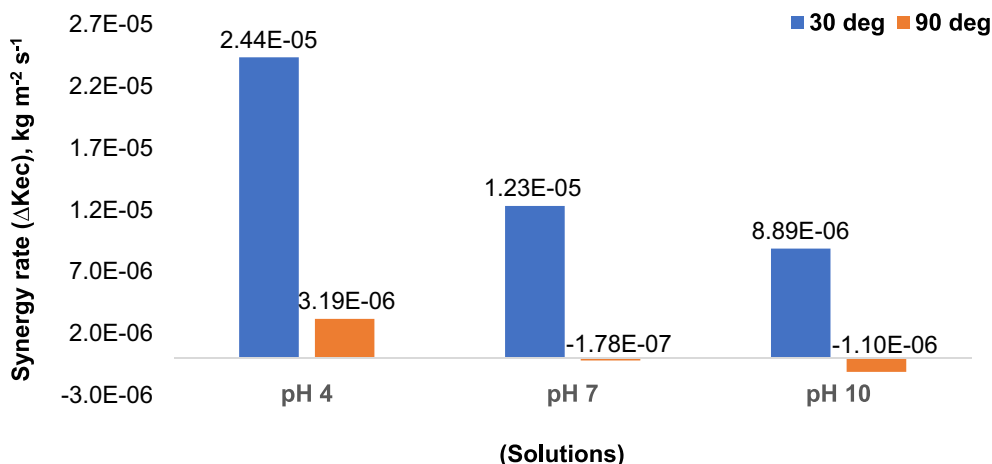

Fig. 4. Effect of synergy in Ta erosion-corrosion with various pH solutions at oblique and normal impact.
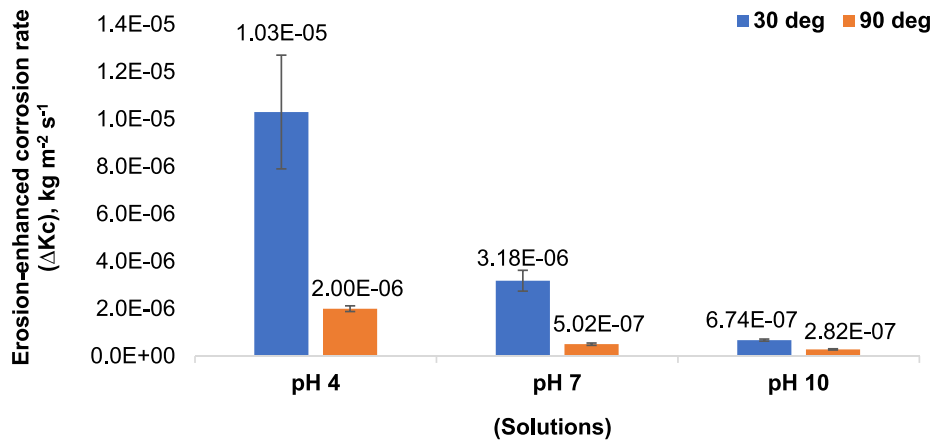
Fig. 5. Ta erosion enhanced corrosion rate in various pH solutions at oblique and normal impact.
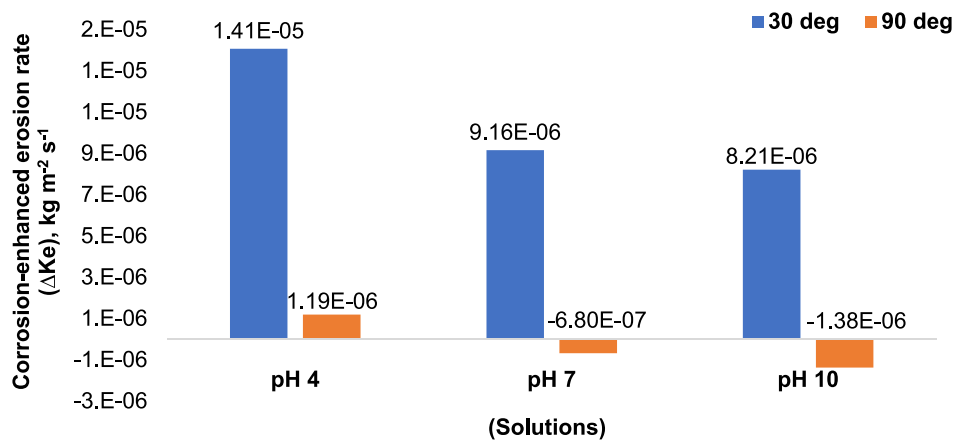

Fig. 6. Ta corrosion enhanced erosion rate in various pH solutions at oblique and normal impact.

Table 5
Summary of calculated mean erosion-corrosion parameters and major contributors of synergy rate (ΔK_{ec}).

Impact angle (°)	pH	K_{ec} (kg m^{-2} s^{-1}) x 10^{-5}	ΔK_{ec} (kg m^{-2} s^{-1}) x 10^{-5}	ΔK_c (kg m^{-2} s^{-1}) x 10^{-5}	ΔK_e (kg m^{-2} s^{-1}) x 10^{-5}	Major Contributor (ΔK_c or ΔK_e)
30	4	3.47 ± 0.2	2.44	1.03 ± 0.2	1.41	Synergistic effect (ΔK_e)
	7	2.27 ± 0.08	1.24	0.32 ± 0.04	0.92	Synergistic effect (ΔK_e)
	10	1.98 ± 0.1	0.89	0.07 ± 0.004	0.82	Synergistic effect (ΔK_e)
	4	1.22 ± 0.2	0.32	0.20 ± 0.01	0.12	Additive effect (ΔK_c)
90	7	0.90 ± 0.06	-0.02	0.05 ± 0.005	-0.07	Antagonistic effect ($-\Delta K_e$)
	10	0.83 ± 0.03	-0.11	0.03 ± 0.003	-0.14	Antagonistic effect ($-\Delta K_e$)

Based on the overall synergy rate (ΔK_{ec}) and its contribution through additive effect (ΔK_c) and synergistic effect (ΔK_e), a brief table summarising the dominant contributor of synergy rate in the erosion-corrosion of Ta is shown in Table 5.

4. Conclusions

The effect of pH and impact angles on the slurry erosion-corrosion behaviour of pure Tantalum (manufactured through PM route) was studied in various corrosive solutions and the following conclusions can be drawn:

1. A marked diminution in the E_{Corr} values (in the range of 400–500 mV) and hence in the corrosion resistance of Ta was observed under the conditions of particle bombardment.
2. Irrespective of the type of corrosive solution (employed in this study), erosion-corrosion rate obtained at 30° impact angle was more than two times than at 90° impact angle. Erosion-corrosion rate was higher at pH 4 as compared to that at pH 7 and pH 10.
3. The erosion-corrosion mechanisms observed consisted of dominating micro-cutting at 30° impact angle. For normal impact angle, plastic deformation leading to lip formation followed by their removal by further particle impacts was found dominating. The corrosion mechanisms included dissolution of the weakened areas due to

plastic deformation in anodic potentials and a continuous removal/formation of passive layers in the passivating potentials.

4. An additive effect (erosion enhanced corrosion rate) was evident at normal impact for pH 4. The antagonistic effect (impairment of erosion by corrosion) was observed for normal impact in pH 7 and pH 10 solutions. The synergistic effect (corrosion enhanced erosion rate) was evident at 30° impact irrespective of pH value.

CRediT authorship contribution statement

J.S. Chouhan: Data Curation, Writing- Original Draft Preparation. **Y.P. Purandare:** Supervision, Research Methodology, Writing - Review & Editing, Visualization. **B.D. Jana:** Conceptualization, Research Methodology, Supervision, Project administration, Funding acquisition; Visualization and Technical Discussion. **A. Dey:** Conceptualization, Supervision, Research Methodology, Help with Metallography, Visualization. **P. Eh. Hovsepian:** Research Methodology, Visualization and Technical Discussion. **D. Jenkins:** Conceptualization, Research Methodology, Visualization and Technical Discussion. **L. Jones:** Conceptualization, Research Methodology, Visualization and Technical Discussion.

Rights retention statement

For the purpose of open access, the author has applied a Creative Commons Attribution (CC BY) licence to any Author Accepted Manuscript version arising from this submission.

Declaration of Competing Interest

- The authors declare the following financial interests/personal relationships which may be considered as potential competing interests: Jitendra Chouhan reports financial support was provided by Rutherford Appleton Laboratory.

Data availability

Data will be made available on request.

Acknowledgement

References

[1] S.M. Cardonne, P. Kumar, C.A. Michaluk, H.D. Schwartz, Tantalum and its alloys, Science (80-.) 13 (1995) 187–194, https://doi.org/10.1126/science.22.559.346.

[2] D.J.S. Findlay, ISIS - Pulsed neutron and muon source, Proc. IEEE Part. Accel. Conf. (2007) 695–699, https://doi.org/10.1109/PAC.2007.4441104.

[3] M.F. Masayoshi Kawai, Kenji Kikuchi, Hiroaki Kurishita, Jing-Feng Li, Fabrication of a tantalum-clad tungsten target for KENS, J. Nucl. Mater. 296 (2001) 312–320, https://doi.org/10.1016/j.jnucmat.2011.11.041.

[4] A.T. Nelson, J.A. O'Toole, R.A. Valicenti, S.A. Maloy, Fabrication of a tantalum-clad tungsten target for LANSCE, J. Nucl. Mater. 431 (2012) 172–184, https://doi.org/10.1016/j.jnucmat.2011.11.041.

[5] A. Dey, L. Jones, Strategies to improve ISIS TS2 target life, J. Nucl. Mater. 506 (2018) 63–70, https://doi.org/10.1016/j.jnucmat.2017.12.044.

[6] G. Marinelli, F. Martina, S. Ganguly, S. Williams, Microstructure, hardness and mechanical properties of two different unalloyed tantalum wires deposited via wire + arc additive manufacture, Int. J. Refract. Met. Hard Mater. 83 (2019), 104974, https://doi.org/10.1016/j.ijrmhm.2019.104974.

[7] I. Hutchings, P. Shipway, Wear by hard particles, in: Tribology, 2nd ed, Elsevier Ltd., 2017, pp. 206–220, https://doi.org/10.1016/b978-0-08-100910-9.00006-4.

[8] J.S. Chouhan, B.D. Jana, Y.P. Purandare, A. Dey, P.E. Hovsepian, D. Jenkins, L. Jones, Preliminary investigation of slurry erosion behaviour of tantalum, Wear. 516–517 (2022) 1–9, https://doi.org/10.1016/j.wear.2022.204605.

[9] K. Yasunaga, H. Watanabe, N. Yoshida, T. Muroga, N. Noda, Correlation between defect structures and hardness in tantalum irradiated by heavy ions, J. Nucl. Mater. 283–287 (2000) 179–182, https://doi.org/10.1016/S0022-3115(00)00354-8.

[10] T. Zaharoni, D. Yunger, N. Mishra, I.G. Segev, A. Kraisel, E. Yahel, G. Makov, MeV proton irradiation damage in Ta: measurements, characterization and comparison to W, J. Nucl. Mater. 553 (2021), 153058, https://doi.org/10.1016/j.jnucmat.2021.153058.

[11] Ian Hutchings, Philip Shipway, Tribology: friction and wear of engineering materials, in: Tribol. Int, 2nd ed, Elsevier Ltd., 2017, pp. 206–231, https://doi.org/10.1016/S0301-679X(98)00079-6.

[12] A.V. Levy, Analytical expressions for erosion and ductile metals, in: Solid Part. Eros. Erosion-Corrosion Mater, 1st ed., ASM International, 1996, pp. 8–9, https://doi.org/10.5860/choice.33-2760.

[13] D. Landolt, S. Mischler, Tribocorrosion of Passive Metals and Coatings, 2011, https://doi.org/10.1533/9780857093738.

[14] R.J.K. Wood, S.P. Hutton, The synergistic effect of erosion and corrosion: trends in published results, Wear. 140 (1990) 387–394, https://doi.org/10.1016/0043-1648(90)90098-U.

[15] M.M. Stack, B.D. Jana, S.M. Abdelrahman, Models and mechanisms of erosion-corrosion in metals, Tribocorrosion Passiv. Met. Coatings. (2011) 153–186, https://doi.org/10.1016/B978-1-84569-966-6.50006-3.

[16] T. Hodgkiess, A. Neville, S. Shrestha, Electrochemical and mechanical interactions during erosion-corrosion of a high-velocity oxy-fuel coating and a stainless steel, Wear. 233–235 (1999) 623–634, https://doi.org/10.1016/S0043-1648(99)00246-X.

[17] Y.P. Purandare, M.M. Stack, P.E. Hovsepian, Velocity effects on erosion-corrosion of CrN/NbN "superlattice" PVD coatings, Surf. Coat. Technol. 201 (2006) 361–370, https://doi.org/10.1016/j.surfcoat.2005.11.143.

[18] G119-09, Standard Guide for Determining Synergism Between Wear and Corrosion, ASTM Int, 2009, pp. 1–7, https://doi.org/10.1520/G0119-09.2.

[19] M. Stern, A.L. Geary, Electrochemical polarization: a theoretical analysis of the shape of polarization curves, J. Electrochem. Soc. 104 (1957) 56–63, https://doi.org/10.1149/1.2428496.

[20] Y. Freeman, P. Lessner, A.J. Kramer, J. Li, E.C. Dickey, J. Koenitzer, L. Mann, Q. Chen, J. Kinard, J. Qazi, Low voltage specific charge (CV/g) loss in tantalum capacitors, J. Electrochem. Soc. 157 (2010) G161, https://doi.org/10.1149/1.3391671.

[21] R.T. Loto, M. Udo, Effect of SiC particle additions on the corrosion resistance, thermodynamic stability and surface morphology of Mg-Al alloy in sulphate and chloride media, Mater. Res. Express. 6 (2019) 1–9, https://doi.org/10.1088/2053-1591/ab273c.

[22] J.G.A. Bitter, A study of erosion phenomena. Part I, Wear. 6 (1963) 5–21, https://doi.org/10.1016/0043-1648(63)90003-6.

[23] J.G.A. Bitter, A study of erosion phenomena. Part II, Wear. 6 (1963) 169–190, https://doi.org/10.1016/0043-1648(63)90073-5.

[24] M. Abedini, H.M. Ghasemi, Synergistic erosion-corrosion behavior of Al-brass alloy at various impingement angles, Wear. 319 (2014) 49–55, https://doi.org/10.1016/j.wear.2014.07.008.

[25] M.D. Bermúdez, F.J. Carrión, G. Martínez-Nicolás, R. López, Erosion-corrosion of stainless steels, titanium, tantalum and zirconium, Wear. 258 (2005) 693–700, https://doi.org/10.1016/j.wear.2004.09.023.

[26] J. Berget, T. Rogne, E. Bardal, Erosion-corrosion properties of different WC-Co-Cr coatings deposited by the HVOF process-influence of metallic matrix composition and spray powder size distribution, Surf. Coat. Technol. 201 (2007) 7619–7625, https://doi.org/10.1016/j.surfcoat.2007.02.032.

[27] D. López, N.A. Falleiros, A.P. Tschiptschin, Corrosion-erosion behaviour of austenitic and martensitic high nitrogen stainless steels, Wear. 263 (2007) 347–354, https://doi.org/10.1016/j.wear.2007.01.053.

[28] M.R. Bateni, J.A. Szpunar, X. Wang, D.Y. Li, Wear and corrosion wear of medium carbon steel and 304 stainless steel, Wear. 260 (2006) 116–122, https://doi.org/10.1016/j.wear.2004.12.037.

[29] H.X. Guo, B.T. Lu, J.L. Luo, Interaction of mechanical and electrochemical factors in erosion-corrosion of carbon steel, Electrochim. Acta 51 (2005) 315–323, https://doi.org/10.1016/j.electacta.2005.04.032.

[30] A. Neville, M. Reyes, H. Xu, Examining corrosion effects and corrosion/erosion interactions on metallic materials in aqueous slurries, Tribol. Int. 35 (2002) 643–650, https://doi.org/10.1016/S0301-679X(02)00055-5.

[31] S.S. Rajahram, T.J. Harvey, R.J.K. Wood, Erosion-corrosion resistance of engineering materials in various test conditions, Wear. 267 (2009) 244–254, https://doi.org/10.1016/j.wear.2009.01.052.

[32] S.S. Rajahram, T.J. Harvey, R.J.K. Wood, Evaluation of a semi-empirical model in predicting erosion-corrosion, Wear. 267 (2009) 1883–1893, https://doi.org/10.1016/j.wear.2009.03.002.

[33] G.A. Zhang, L.Y. Xu, Y.F. Cheng, Investigation of erosion-corrosion of 3003 aluminum alloy in ethylene glycol-water solution by impingement jet system, Corros. Sci. 51 (2009) 283–290, https://doi.org/10.1016/j.corsci.2008.10.026.

[34] M. Pourbaix, Atlas of electrochemical equilibria in aqueous solutions, in: NACE Int. Cebelcor, Second, NACE, 1974, p. 251, https://doi.org/10.1016/0022-0728(67)80059-7.

[35] A. Robin, J.L. Rosa, Corrosion behavior of niobium, tantalum and their alloys in hot hydrochloric and phosphoric acid solutions, Int. J. Refract. Met. Hard Mater. 18 (2000) 13–21, https://doi.org/10.1016/S0263-4368(99)00034-7.

[36] S.C. Kuiry, S. Seal, W. Fei, J. Ramsdell, V.H. Desai, Y. Li, S.V. Babu, B. Wood, Effect of pH and H2O2 on Ta chemical mechanical planarization, J. Electrochem. Soc. 150 (2003) 36–43, https://doi.org/10.1149/1.1528202.

[37] A. Robin, Corrosion behaviour of tantalum in sodium hydroxide solutions, J. Appl. Electrochem. 33 (2003) 37–42, https://doi.org/10.1023/A:1022982320438.

[38] I. Mickova, Electrochemical behavior of tantalum in potassium hydroxide solutions, J. Electrochem. Sci. Eng. 8 (2018) 291–301, https://doi.org/10.5599/jese.537.